RETHINKING KNOWLEDGE GRAPH PROPAGATION FOR ZERO-SHOT LEARNING

Anonymous authors
Paper under double-blind review

ABSTRACT

Graph convolutional neural networks have recently shown great potential for the task of zero-shot learning. These models are highly sample efficient as related concepts in the graph structure share statistical strength allowing generalization to new classes when faced with a lack of data. However, we find that the extensive use of Laplacian smoothing at each layer in current approaches can easily dilute the knowledge from distant nodes and consequently decrease the performance in zero-shot learning. In order to still enjoy the benefit brought by the graph structure while preventing the dilution of knowledge from distant nodes, we propose a Dense Graph Propagation (DGP) module with carefully designed direct links among distant nodes. DGP allows us to exploit the hierarchical graph structure of the knowledge graph through additional connections. These connections are added based on a node's relationship to its ancestors and descendants. A weighting scheme is further used to weigh their contribution depending on the distance to the node. Combined with finetuning of the representations in a two-stage training approach our method outperforms state-of-the-art zero-shot learning approaches.

1 INTRODUCTION

With the ever-growing supply of image data, from an ever-expanding number of classes, there is an increasing need to use prior knowledge to classify images from unseen classes into correct categories based on semantic relationships between seen and unseen classes. This task is called zero-shot image classification. To obtain satisfactory performance on this task, it is crucial to model precise class relationships based on prior class knowledge. Previously prior knowledge has been incorporated in form of semantic descriptions of classes, such as attributes (Akata et al., 2015; Romera-Paredes & Torr, 2015; Long et al., 2017) or word embeddings (Socher et al., 2013; Frome et al., 2013; Li et al., 2017), or by using semantic relations such as knowledge graphs (Palatucci et al., 2009; Rohrbach et al., 2011; Salakhutdinov et al., 2011; Lu, 2016). Approaches that use knowledge graphs are less-explored and generally are based on the assumption that unknown classes can exploit similarity to known classes. Recently the benefit of hybrid approaches that combine knowledge graph and semantic class descriptions has been illustrated (Wang et al., 2018).

The current state-of-the-art approach Wang et al. (2018) processes knowledge graphs by making use of recent developments in applying neural network techniques to non-euclidean spaces, such as graph and manifold spaces (Bronstein et al., 2017). A deep graph convolutional neural network (GCN) (Kipf & Welling, 2017) is used and the problem is phrased as weight regression, where the GCN is trained to regress classifier weights for each class. GCNs balance model complexity and expressiveness with a simple scalable model relying on the idea of message passing, i.e. nodes pass knowledge to their neighbors. However, these models were originally designed for classification tasks, albeit semi-supervised, an arguably simpler task than regression. In recent work, it has been shown that GCNs perform a form of Laplacian smoothing, where feature representations will become more similar as depth increases leading to easier classification (Li et al., 2018). In the regression setting, instead, the aim is to exchange information between nodes in the graph and extensive smoothing is not desired as it dilutes information and does not allow for accurate regression. For instance, in a connected graph all features in a GCN with n layers will converge to the same representation as $n \to \infty$ under some conditions, hence washing out all information (Li et al., 2018).

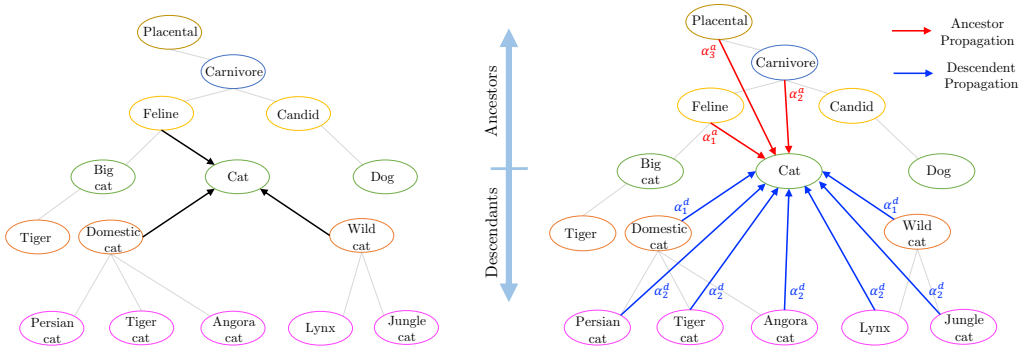

(a) Graph Propagation (b) Dense Graph Propagation

Figure 1: a) Illustration of graph propagation in a GCN (Kipf & Welling, 2017) for node 'Cat'. Here, graph propagation represents the knowledge that a node receives in a single layer for previous approaches. b) Proposed dense graph propagation for node 'Cat'. The node receives knowledge from all its descendants during the descendant phase (blue arrows) and its ancestors during the ancestor phase (red arrows). This leads to a densely connected graph where knowledge can directly propagate between related nodes. Weights α_k are used to weigh nodes that are k-hops away from a given node.

We, therefore, argue that this approach is not ideal for the task of zero-shot learning and that the number of layers in the graph should be small in order to avoid smoothing. We illustrate this phenomenon in practice, by showing that a shallow GCN consistently outperforms previously reported results. We employ a model-of-models framework by training the method to predict a set of logistic regression classifier for each class on top of a set of extracted features produced by a CNN. Choosing a small number of layers, however, has the effect that knowledge will not propagate well through the graph. A 1-layer GCN for instance only considers neighbors that are two hops away in the graph such that only immediate neighbors influence a given node. Thus, we propose a dense connectivity scheme, where nodes are connected directly to descendants/ancestors in order to include distant information. These connections allow us to propagate information without many smoothing operations but leads to the problem that all descendants/ancestors are weighed equally when computing the regression weight vector for a given class. However, intuitively, nodes closer to a given node should have higher importance. To remedy this, we extend this framework by adding a weighting scheme that considers the distance between nodes in order to weigh the contribution of different nodes. Making use of shared weights based on the distance also has the advantage that it only adds a minimal amount of additional parameters, is computationally efficient, and provides a balance between increasing flexibility of the model and keeping it restrictive enough to allow good predictions for the nodes of the unseen classes. Figure 1 illustrates the difference in the way knowledge is propagated in this proposed Dense Graph Propagation (DGP) module compared to a GCN layer.

To allow the feature extraction stage of the pre-trained CNN to adjust to the newly learned classifiers we propose a two-phase training scheme. In the first step, the DGP is trained to predict the last layer CNN weights. In the second phase, we replace the last layer weights of the CNN with the weights predicted by the DGP, freeze the weights and finetune the remaining weights of the CNN by optimizing the cross entropy classification loss on the seen classes.

Our contributions can be summarized as follows. We present

- an analysis of our intuitions for zero-shot learning and illustrate how these intuitions can be combined to design a DGP that outperforms previous zero-shot learning results.[1]
- our DGP module, which explicitly exploits the hierarchical structure of the knowledge graph in order to perform zero-shot learning by more efficiently propagating knowledge through the proposed dense connectivity structure.
- a novel weighting scheme for the dense model based on the distance between nodes.
- experimental results on various splits of the 21K ImageNet dataset, a commonly used large-scale dataset for zero-shot learning. We obtain relative improvements of more than 50% over the previously reported best results.

[1]The source code for the experiments performed in this paper is available at: `https://www.dropbox.com/s/jz3kff4qdpcooq0/Code.zip?dl=0`.

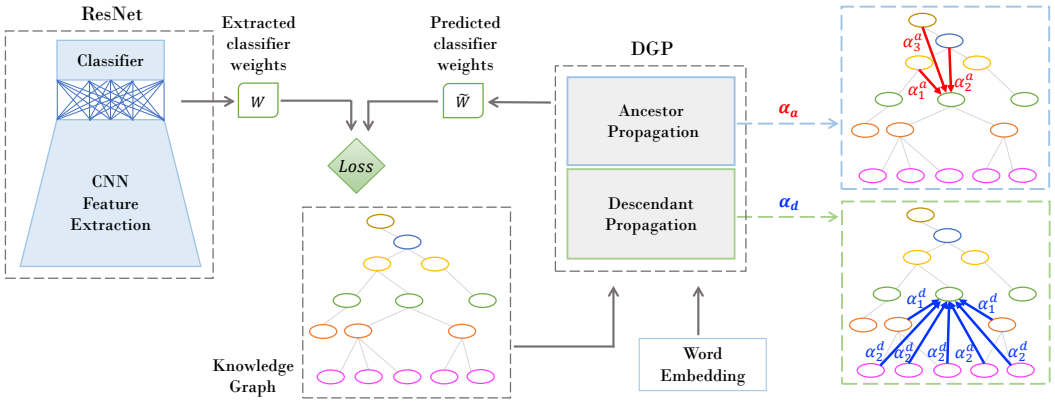

Figure 2: DGP is trained to predict classifier weights W for each node/class in a graph. These weights are extracted from the final layer of a pre-trained ResNet. The graph is constructed from a knowledge graph and each node is represented by its word embedding (semantic information). The network consists of two phases, a descendant phase where each node receives knowledge form its descendants and an ancestor phase, where it receives knowledge from its ancestors.

2 Related Work

Graph convolutional networks are a class of graph neural networks, based on local graph operators (Bruna et al., 2013; Defferrard et al., 2016; Kipf & Welling, 2017). Their advantage is that their graph structure allows the sharing of statistical strength between classes making these methods highly sample efficient. After being introduced in Bruna et al. (2013), they were extended with an efficient filtering approach based on recurrent Chebyshev polynomials, reducing their computational complexity to the equivalent of the commonly used CNNs in image processing operating on regular grids (Defferrard et al., 2016). Kipf & Welling (2017) further proposed simplifications to improve scalability and robustness and applied their approach to semi-supervised learning on graphs. Their approach is termed graph convolutional network (GCN).

Zero-shot learning has in recent years been considered from various set of viewpoints such as manifold alignment (Deutsch et al., 2017; Li et al., 2017), linear auto-encoder (Kodirov et al., 2017), and low-rank embedded dictionary learning approaches (Ding et al., 2017), using semantic relationships based on attributes (Misra et al., 2017; Socher et al., 2013; Frome et al., 2013) and relations in knowledge graphs (Wang et al., 2018; Mensink et al., 2012; Rohrbach et al., 2011; Palatucci et al., 2009). One of the early works (Larochelle et al., 2008) proposed a method based on the idea of a model-of-model class approach, where a model is trained to predict models based on their description. Each class is modeled as a function of its description. This idea has recently been used in another work in Wang et al. (2018), the work most similar to our own, where a graph convolutional neural network is trained to predict logistic regression classifiers on top of pre-trained CNN features. Wang et al. (2018) proposed to use GCNs (Kipf & Welling, 2017) to predict a set of logistic regression classifiers, one for each class, on top of pre-trained CNN features in order to predict unseen classes. Their approach has yielded impressive performance on a set of zero-shot learning tasks and can, to the author's knowledge be considered to be the current state-of-the-art.

3 Approach

Here we first formalize the problem of zero-shot learning and provide information on how a GCN model can be utilized for the task of zero-shot learning and then describe our proposed model DGP. Our zero-shot learning framework to address this task is illustrated in Figure 2. We train our DGP, to predict the last layer CNN weights for each class/concept.

3.1 Zero-shot learning

Zero-shot classification aims to predict the class labels of a set of test data points to a set of classes $\mathcal{C}_{te}$. However, unlike in common supervised classification, the test data set points have to be assigned

to previously unseen classes, given a L dimensional semantic representation vector $z \in \mathbb{R}^L$ per class $\mathcal{C}$ and a set of training data points $\mathcal{D}_{tr} = \{(\vec{X}_i, c_i)\, i = 1, ..., N\}$, where $\vec{X}_i$ denotes the i-th training image and $c_i \in \mathcal{C}_{tr}$ the corresponding class label. Here $\mathcal{C}$ denotes the set of all classes and $\mathcal{C}_{te}$ and $\mathcal{C}_{tr}$ the test and training classes, respectively. Note that training and test classes are disjoint $\mathcal{C}_{te} \cap \mathcal{C}_{tr} = \emptyset$ for the zero-shot learning task. In this work, we perform zero-shot classification by using the word embedding of the class labels and the knowledge graph to predict classifiers for each unknown class in form of last layer CNN weights.

3.2 Graph Convolutional Networks for Zero-Shot Learning

Given a graph with N nodes and with C input features per node, $X \in \mathbb{R}^{N \times C}$ is used to denote the feature matrix. Here each node represents a distinct concept/class in the classification task and each concept is represented by a word vector of the class name. The connections between the classes in the knowledge graph are encoded in form of a symmetric adjacency matrix $A \in \mathbb{R}^{N \times N}$, which also includes self-loops. We employ a simple propagation rule to perform convolutions on the graph

$$H^{(l+1)} = \sigma\left(D^{-1}AH^{(l)}\Theta^{(l)}\right) , \tag{1}$$

where $H^{(l)}$ represents the activations in the l^{th} layer and $\Theta \in \mathbb{R}^{C \times F}$ denotes the trainable weight matrix for layer l. For the first layer, $H^{(0)} = X$. $\sigma(\cdot)$ denotes a nonlinear activation function, in our case a Leaky ReLU. $D_{ii} = \sum_j A_{ij}$ is a degree matrix $D \in \mathbb{R}^{N \times N}$, which normalizes rows in A to ensure that the scale of the feature representations is not modified by A. Similar to previous work done on graph convolutional neural networks, this propagation rule can be interpreted as a spectral convolution (Kipf & Welling, 2017).

The model is trained to predict the classifier weights for the seen classes by optimizing the loss

$$\mathcal{L} = \frac{1}{2M}\sum_{i=1}^{M}\sum_{j=1}^{L}(W_{i,j} - \widetilde{W}_{i,j})^2 , \tag{2}$$

where $\widetilde{W} \in \mathbb{R}^{M \times L}$ denotes the prediction of the GCN for the known classes and therefore corresponds to the M rows of the GCN output, which correspond to the training classes. M denotes the number of training classes and L denotes the dimensionality of the weight vectors. The ground truth weights are obtained by extracting the last layer weights of a pre-trained CNN and denoted as $W \in \mathbb{R}^{M \times L}$. During testing, the features of new images are extracted from the CNN and the classifiers predicted by the GCN are used to classify the features.

3.3 Dense Graph Propagation Module

Our DGP for zero-shot learning aims to utilize the hierarchical graph structure for the zero-shot learning task and avoids the dilution of knowledge by intermediate nodes. This is achieved using a dense graph connectivity scheme consisting of two phases, namely the descendant propagation phase and the ancestor propagation phase. This two-phase approach further enables the model to learn separate relations between a node and its ancestors and a node and its descendants. Appendix B provides empirical evidence for this choice. Unlike in the GCN, we do not use the knowledge graph relations directly as an adjacency graph to include information from neighbors further away. We do therefore not suffer from the problem of knowledge being washed out due to averaging over the graph. Instead, we introduce two separate connectivity patterns, one where nodes are connected to all their ancestors and one where nodes are connected to all descendants. We utilize two adjacency matrices $A_a \in \mathbb{R}^{N \times N}$ that denotes the connections from nodes to their ancestors and adjacency matrix A_d that denotes the connections from nodes to their descendants. Note, $A_d = A_a^T$. Unlike in previous approaches, this connectivity pattern allows nodes direct access to knowledge in their extended neighborhood as opposed to knowledge that has been modified by intermediate nodes. Note that both these adjacency matrices include self-loops. The connection pattern is illustrated in Figure 1. The same propagation rule as in Equation 1 is applied consecutively for the two connectivity patterns leading to the overall DGP propagation rule

$$H = \sigma\left(D_a^{-1}A_a\sigma\left(D_d^{-1}A_dX\Theta_d\right)\Theta_a\right) . \tag{3}$$

Distance weighting scheme In order to allow DGP to weigh the contribution of various neighbors in the dense graph, we propose a weighting scheme that weighs a given nodes neighbors based on the graph distance from the node. Note, the distance is computed on the knowledge graph and not the dense graph. We use $w^a = \{w_i^a\}_{i=0}^K$ and $w^d = \{w_i^d\}_{i=0}^K$ to denote the weights for the ancestor and the descendant propagation phase, respectively. w_i^a and w_i^d correspond to weights for nodes that are i hops away from the given node. w_0^a, w_0^d correspond to self-loops and w_K^a, w_K^d correspond to the weights for nodes further than $K-1$ hops away. We normalize the weights using a softmax function $\alpha_k^a = \text{softmax}(w_k^a) = \frac{\exp(w_k^a)}{\sum_{i=0}^K \exp(w_i^a)}$. Similarly, $\alpha_k^d = \text{softmax}(w_k^d)$. The weighted propagation rule in Equation 3 becomes

$$H = \sigma\left(\sum_{k=0}^{K} \alpha_k^a D_k^{a^{-1}} A_k^a \sigma\left(\sum_{k=0}^{K} \alpha_k^d D_k^{d^{-1}} A_k^d X \Theta_d\right)\Theta_a\right) , \tag{4}$$

where A_k^a and A_k^d is used to denote the parts of the adjacency matrices that only contains the k-hop edges for the ancestor and descendant propagation phase, respectively. D_k^a and D_k^d are the corresponding degree matrices for A_k^a and A_k^d.

3.4 FINETUNING

Training of the proposed model is done in two stages, where the first stage trains the DGP to predict the last layer weights of a pre-trained CNN using Equation 2. Note, $\widetilde{W}$, in this case, contains the M rows of H, which correspond to the training classes. In order to allow the feature representation of the CNN to adapt to the new class classifiers, we train the CNN by optimizing the cross-entropy classification loss on the seen classes in a second stage. During this stage, the last layer weights are fixed to the predicted weights of the training classes in the DGP and only the feature representation is updated. This can be viewed as utilizing the DGP as a constraint for the CNN, as we indirectly incorporate the graph information in order to constrain the CNN output space.

3.5 TRAINING DETAILS

We use a ResNet-50 (He et al., 2015) model that has been pre-trained on the ImageNet 2012 dataset. Following Wang et al. (2018), we use the GloVe text model (Pennington et al., 2014), which has been trained on the Wikipedia dataset, as the feature representation of our concepts in the graph. The DGP model consists of two layers as illustrated in Equation 3 with feature dimensions of 2048 and the final output dimension corresponds to the number of weights in the last layer of the ResNet-50 architecture, 2049 for weights and bias. Following the observation of Wang et al. (2018), we perform L2-Normalization on the outputs as it regularizes the outputs into similar ranges. Similarly, we also normalize the ground truth weights produced by the CNN. We further make use of Dropout (Srivastava et al., 2014) with a dropout rate of 0.5 in each layer. The model is trained for 3000 epochs with a learning rate of 0.001 and weight decay of 0.0005 using Adam (Kingma & Ba, 2015). We make use of leaky ReLUs with a negative slope of 0.2. The number of values per phase K was set to 4 as additional weights had diminishing returns. The proposed DGP model is implemented in PyTorch (Paszke et al., 2017) and training and testing are performed on a GTX 1080Ti GPU. Finetuning is done for 20 epochs using SGD with a learning rate of 0.0001 and momentum of 0.9.

4 EXPERIMENTS

We performed a comparative evaluation of the DGP against previous state-of-the-art on the ImageNet dataset (Deng et al., 2009), the largest commonly used dataset for zero-shot learning. In our work, we follow the train/test split suggested by Frome et al. (2013), who proposed to use the 21K ImageNet dataset for zero-shot evaluation. They define three tasks in increasing difficulty, denoted as "2-hops", "3-hops" and "All". Hops refer to the distance that classes are away from the ImageNet 2012 1K classes in the ImageNet hierarchy and thus is a measure of how far unseen classes are away from seen classes. "2-hops" contains all the classes within two hops from the seen classes and consists of roughly 1.5K classes, while "3-hops" contains about 7.8K classes. "All" contains close to 21K classes. None of the classes are contained in the ImageNet 2012 dataset, which was used to pre-train the ResNet-50 model. Mirroring the experiment setup in Frome et al. (2013); Norouzi et al. (2014);

Wang et al. (2018) we further evaluate the performance when training categories are included as potential labels. Note that since the only difference is the number of classes during testing, the model does not have to be retrained. We denote the splits as "2-hops+1K", "3-hops+1K", "All+1K".

4.1 COMPARING APPROACHES

We compare our DGP to the following approaches: **Devise** (Frome et al., 2013) linearly maps visual information in form of features extracted by a convolutional neural network to the semantic word-embedding space. The transformation is learned using a hinge ranking loss. Classification is performed by assigning the visual features to the class of the nearest word-embedding. **ConSE** (Norouzi et al., 2014) projects image features into a semantic word embedding space as a convex combination of the T closest seen classes semantic embedding weighted by the probabilities that the image belongs to the seen classes. The probabilities are predicted using a pre-trained convolutional classifier. Similar to Devise, ConSE assigns images to the nearest classes in the embedding space. **EXEM** (Changpinyo et al., 2017) creates visual class exemplars by averaging the PCA projections of images belonging to the same seen class. A kernel-based regressor is then learned to map a semantic embedding vector to the class exemplar. For zero-shot learning visual exemplars can be predicted for the unseen classes using the learned regressor and images can be assigned using nearest neighbor classification. **SYNC** (Changpinyo et al., 2016) aligns a semantic space (e.g., the word-embedding space) with a visual model space, adds a set of phantom object classes in order to connect seen and unseen classes, and derives new embeddings as a convex combination of these phantom classes. **GCNZ** (Wang et al., 2018) represents the current state of the art and is the approach most related to our proposed DGP. A GCN is trained to predict last layer weights of a convolutional neural network.

Guided by experimental evidence (see Appendix C) and our intuition that extensive smoothing is a disadvantage for the weight regression in the task of zero-shot learning we add as another baseline, a single-hidden-layer GCN (**SGCN**) with non-symmetric normalization ($D^{-1}A$) (as defined in Equation 1). Note, GCNZ made use of a symmetric normalization ($D^{-1/2}AD^{-1/2}$) but our experimental evaluation indicates that the difference is negligible (see Appendix D). It further yields a better baseline as our proposed DGP also utilizes the non-symmetric normalization. As DGP, our SGCN model makes use of the proposed two-stage finetuning approach.

4.2 COMPARISON TO STATE-OF-THE-ART METHODS: IMAGENET

Quantitative results for the comparison on the ImageNet datasets are shown in Table 1. Compared to previous results such as ConSE (Changpinyo et al., 2016), EXEM (Changpinyo et al., 2017), and GCNZ (Wang et al., 2018) our proposed methods outperform the previous results with a considerable margin, achieving, for instance, more than 50% relative improvement for Top-1 accuracy on the 21K ImageNet "All" dataset. We observe that our methods especially outperform the baseline models on the "All" task, illustrating the potential of our methods to more efficiently propagate knowledge. DGP also achieves consistent improvements over the SGCN model. We observed that finetuning consistently improved performance for both models in all our experiments. Ablation studies that highlight the impact of finetuning and weighting of neighbors for the 2-hop scenario can be found in Table 3. DGP(-wf) is used to denote the accuracy that is achieved after training the DGP model without weighting (adding no weights in Equation 4) and without finetuning. DGP(-w) and DGP(-f) are used to denote the results for DGP without weighting and DGP without finetuning, respectively. We further report the accuracy achieved by the SGCN model without finetuning (SGCN(-f)). We observe that the proposed weighting scheme, which allows distant neighbors to have less impact, is crucial for the dense approach. Further, finetuning the model consistently leads to improved results. The results are stable over multiple runs and we include variance information for multiple runs in Appendix E.

Qualitative results of DGP and the SGCN are shown in Figure 3. Example images from unseen test classes are displayed and we compare the results of our proposed DGP and the SGCN to results produced by a pre-trained ResNet. Note, ResNet can only predict training classes while the others predict classes not seen in training. For comparison, we also provide results for our re-implementation of GCNZ. We observe that the SGCN and DGP generally provide coherent top-5 results. All methods struggle to predict the *opener* and tend to predict some type of *plane* instead, however, DGP does include *opener* in the top-5 results. We further observe that the prediction task on this dataset for

Table 1: Top-k accuracy for the different models on the ImageNet dataset. Accuracy when only testing on unseen classes. Results indicated with *, †, and ‡ are taken from Changpinyo et al. (2016), Changpinyo et al. (2017), and Wang et al. (2018), respectively.

Test set	Model	Hit@k (%) 1	2	5	10	20
2-hops	ConSE*	8.3	12.9	21.8	30.9	41.7
	SYNC*	10.5	17.7	28.6	40.1	52.0
	EXEM†	12.5	19.5	32.3	43.7	55.2
	GCNZ‡	19.8	33.3	53.2	65.4	74.6
	SGCN (ours)	26.2	40.4	60.2	71.9	81.0
	DGP (ours)	**26.6**	**40.7**	**60.3**	**72.3**	**81.3**
3-hops	ConSE*	2.6	4.1	7.3	11.1	16.4
	SYNC*	2.9	4.9	9.2	14.2	20.9
	EXEM†	3.6	5.9	10.7	16.1	23.1
	GCNZ‡	4.1	7.5	14.2	20.2	27.7
	SGCN (ours)	6.0	10.4	18.9	27.2	36.9
	DGP (ours)	**6.3**	**10.7**	**19.3**	**27.7**	**37.7**
All	ConSE*	1.3	2.1	3.8	5.8	8.7
	SYNC*	1.4	2.4	4.5	7.1	10.9
	EXEM†	1.8	2.9	5.3	8.2	12.2
	GCNZ‡	1.8	3.3	6.3	9.1	12.7
	SGCN (ours)	2.8	4.9	9.1	13.5	19.3
	DGP (ours)	**3.0**	**5.0**	**9.3**	**13.9**	**19.8**

Table 2: Top-k accuracy for the different models on the ImageNet dataset. Accuracy when testing on seen and unseen classes. Results indicated with ††, ‡‡, and ‡ are taken from Frome et al. (2013), Norouzi et al. (2014), and Wang et al. (2018), respectively.

Test set	Model	Hit@k (%) 1	2	5	10	20
2-hops+1K	DeViSE††	0.8	2.7	7.9	14.2	22.7
	ConSE‡‡	0.3	6.2	17.0	24.9	33.5
	ConSE‡	0.1	11.2	24.3	29.1	32.7
	GCNZ‡	9.7	20.4	42.6	57.0	68.2
	SGCN (ours)	**11.9**	**27.0**	**50.8**	65.1	75.9
	DGP (ours)	10.3	26.4	50.3	**65.2**	**76.0**
3-hops+1K	DeViSE††	0.5	1.4	3.4	5.9	9.7
	ConSE‡‡	0.2	2.2	5.9	9.7	14.3
	ConSE‡	0.2	3.2	7.3	10.0	12.2
	GCNZ‡	2.2	5.1	11.9	18.0	25.6
	SGCN (ours)	**3.2**	**7.1**	**16.1**	24.6	34.6
	DGP (ours)	2.9	**7.1**	**16.1**	**24.9**	**35.1**
All+1K	DeViSE††	0.3	0.8	1.9	3.2	5.3
	ConSE‡‡	0.2	1.2	3.0	5.0	7.5
	ConSE‡	0.1	1.5	3.5	4.9	6.2
	GCNZ‡	1.0	2.3	5.3	8.1	11.7
	SGCN (ours)	**1.5**	**3.4**	7.8	12.3	18.2
	DGP (ours)	1.4	**3.4**	**7.9**	**12.6**	**18.7**

zero-shot learning is difficult as it contains classes of fine granularity, such as many different types of squirrels, planes, and furniture. Additional examples are provided in the appendix.

Testing including training classifiers. Following the example of (Frome et al., 2013; Norouzi et al., 2014; Wang et al., 2018), we also report the results when including both training labels and testing labels as potential labels during classification of the zero-shot examples. Results are shown in Table 2. For the baselines, we include two implementations of ConSE, one that uses AlexNet as a backbone (Norouzi et al., 2014) and one that uses ResNet-50 (Wang et al., 2018). Compared to Table 1, we observe that the accuracy is considerably lower, but the SGCN and DGP still outperform the previous state-of-the-art approach GCNZ. SGCN outperforms DGP for low k in the Top-k accuracy measure especially for the 2-hops setting, while DGP outperforms SGCN for larger k. We observe that DGP tends to favor prediction to the closest training classes for its Top-1 prediction (see Table 4). However, this is not necessarily a drawback and is a well-known tradeoff (Chao et al., 2016) between performing well on the unseen classes and the seen classes, which are not considered in this setting. In the next paragraph, we will evaluate the model's performance on the seen classes. This tradeoff can be controlled by including a novelty detector, which predicts if an image comes from the seen or unseen classes as done in Socher et al. (2013) and then assigns it to the zero-shot classifier or a classifier trained on the seen classes. Another approach is calibrated stacking (Chao et al., 2016), which rescales the prediction scores of the known classes.

Zero-shot learning models should perform well not only on unseen but also on seen classes. To put the zero-shot performance into perspective, we perform experiments where we analyze how the model's performance on the original 1000 seen classes is affected by domain shift as additional unseen classes (all 2-hop classes) are introduced. Table 4 shows the results when the model is tested on the validation dataset from ImageNet 2012. We compare the performance to our re-implementation of the GCNZ model with ResNet-50 backbone and also the performance from the original ResNet-50 model, which is trained only on the seen classes. It can be observed that both our methods outperform GCNZ on Hit@1 and Hit@2 accuracy.

Analysis of weighting scheme In order to validate our intuition that weighting allows our approach to weigh distance neighbors less, we can inspect the learned weighting. For the first stage the weights are

ResNet: baboon, langur, koala, macaque, madagascar cat
GCNZ: phalanger, kangaroo, lemur, marsupial, **tree squirrel**
SGCN: phalanger, kangaroo,**tree squirrel**, lemur, tree wallaby
DGP: **tree squirrel**, kangaroo, phalanger, lemur, tree wallaby

ResNet: sea lion, oystercatcher, king penguin, ruddy turnstone, meerkat
GCNZ: pelagic bird, wandering albatross, **penguin**, black-footed albatross, california sea lion
SGCN: **penguin**, california sea lion, steller sea lion, south american sea lion, australian sea lion
DGP: **penguin**, california sea lion, south american sea lion, hoary marmot, yellowbelly marmot

ResNet: plane, shoe shop, hook, sundial, electric fan
GCNZ: fastener, block plane, jointer, dovetail plane, scrub plane
SGCN: dovetail plane, beading plane, jointer, circular plane, block plane
DGP: circular plane, dovetail plane, **opener**, jointer, router plane

ResNet: bookcase, entertainment center, library, file, comic book
GCNZ: wall unit, furniture, secretary, davenport, writing desk
SGCN: furniture, office furniture, dining-room table, wall unit, writing desk
DGP: furniture, office furniture, chest of drawers, **cabinet**, wall unit

Figure 3: Qualitative result comparison on Imagenet. The correct class is highlighted in bold. We report the top-5 classification results.

$0.244, 0.476, 0.162, 0.060, 0.058$ and for the second (final) stage $0.493, 0.322, 0.097, 0.047, 0.041$. Note, the first value corresponds to self-attention, the second to the 1-hop neighbors, and so forth. For the first stage, ancestors aggregate information mainly from their immediate descendants to later distribute it to their descendants. Further, we observe that distant neighbors have less impact in the final stage.

Table 3: Results of the ablation experiments on the 2-hops dataset. (-f), (-w), and (-wf) indicate models without finetuning, weighting and without both weighting and finetuning, respectively.

Test set	Model	Hit@k (%) 1	2	5	10	20
2-hops	SGCN(-f)	24.8	38.3	57.5	69.9	79.6
	DGP(-wf)	23.8	36.9	56.2	69.1	78.6
	DGP(-f)	24.6	37.8	56.9	69.6	79.3
	DGP(-w)	25.4	39.5	59.9	72.0	80.9
	SGCN (ours)	26.2	40.4	60.2	71.9	81.0
	DGP (ours)	**26.6**	**40.7**	**60.3**	**72.3**	**81.3**

Table 4: Performance on the seen ImageNet classes. ResNet represents ideal performance as it only predicts known classes.

Model	Hit@k (%) 1	2	5	10
ResNet	75.1	85.5	92.7	95.7
GCNZ (us)	38.3	62.9	82.3	89.8
SGCN (ours)	49.1	68.7	**83.9**	**89.4**
DGP (ours)	**54.6**	**69.7**	83.8	89.1

Scalability. To obtain good scalability it is important that the adjacency matrix A is a sparse matrix so that the complexity of computing $D^{-1}AX\Theta$ is linearly proportional to the number of edges present in A. Our approach utilizes the structure of knowledge graphs, where entities only have few ancestors and descendants, to ensure this. The adjacency matrix for the ImageNet hierarchy used in our experiments, for instance, has a density of 9.3×10^{-5}, while our dense connections only increase the density of the adjacency matrix to 19.1×10^{-5}. With regards to the number of parameters, the SGCN consist of 4,810,752 weights. DGP increases the number of trainable parameters by adding $2 \times (K+1)$ additional weights. However, as $K = 4$ in our experiments, this difference in the number of parameters is negligible.

5 Conclusion

In contrast to previous approaches using graph convolutional neural networks for zero-shot learning, we illustrate that the task of zero-shot learning benefits from shallow networks. Further, to avoid the lack of information propagation between distant nodes in shallow models, we propose DGP, which exploits the hierarchical structure of the knowledge graph by adding a dense connection scheme. Experiments illustrate the ability of the proposed methods, outperforming previous state-of-the-art methods for zero-shot learning. In future work, we aim to investigate the potential of more advanced weighting mechanisms to further improve the performance of DGP compared to the SGCN. The inclusion of additional semantic information for settings where these are available for a subset of nodes is another future direction.

REFERENCES

Zeynep Akata, Scott Reed, Daniel Walter, Honglak Lee, and Bernt Schiele. Evaluation of output embeddings for fine-grained image classification. In *Proceedings of the IEEE Conference on Computer Vision and Pattern Recognition*, pp. 2927–2936, 2015.

Michael M Bronstein, Joan Bruna, Yann LeCun, Arthur Szlam, and Pierre Vandergheynst. Geometric deep learning: going beyond euclidean data. *IEEE Signal Processing Magazine*, 34(4):18–42, 2017.

Joan Bruna, Wojciech Zaremba, Arthur Szlam, and Yann LeCun. Spectral networks and locally connected networks on graphs. *arXiv preprint arXiv:1312.6203*, 2013.

Soravit Changpinyo, Wei-Lun Chao, Boqing Gong, and Fei Sha. Synthesized classifiers for zero-shot learning. In *Proceedings of the IEEE Conference on Computer Vision and Pattern Recognition*, pp. 5327–5336, 2016.

Soravit Changpinyo, Wei-Lun Chao, and Fei Sha. Predicting visual exemplars of unseen classes for zero-shot learning. In *Proceedings of the IEEE Conference on Computer Vision and Pattern Recognition*, pp. 3476–3485, 2017.

Wei-Lun Chao, Soravit Changpinyo, Boqing Gong, and Fei Sha. An empirical study and analysis of generalized zero-shot learning for object recognition in the wild. In *European Conference on Computer Vision*, pp. 52–68. Springer, 2016.

Michaël Defferrard, Xavier Bresson, and Pierre Vandergheynst. Convolutional neural networks on graphs with fast localized spectral filtering. In *Advances in Neural Information Processing Systems*, pp. 3844–3852, 2016.

Jia Deng, Wei Dong, Richard Socher, Li-Jia Li, Kai Li, and Li Fei-Fei. Imagenet: A large-scale hierarchical image database. In *Proceedings of the IEEE Conference on Computer Vision and Pattern Recognition*, pp. 248–255, 2009.

Shay Deutsch, Soheil Kolouri, Kyungnam Kim, Yuri Owechko, and Stefano Soatto. Zero shot learning via multi-scale manifold regularization. In *Proceedings of the IEEE Conference on Computer Vision and Pattern Recognition*, pp. 7112–7119, 2017.

Zhengming Ding, Ming Shao, and Yun Fu. Low-rank embedded ensemble semantic dictionary for zero-shot learning. In *Proceedings of the IEEE Conference on Computer Vision and Pattern Recognition*, pp. 2050–2058, 2017.

Andrea Frome, Greg S Corrado, Jon Shlens, Samy Bengio, Jeff Dean, Tomas Mikolov, et al. Devise: A deep visual-semantic embedding model. In *Advances in Neural Information Processing Systems*, pp. 2121–2129, 2013.

Kaiming He, Xiangyu Zhang, Shaoqing Ren, and Jian Sun. Deep residual learning for image recognition. *arXiv preprint arXiv:1512.03385*, 2015.

Diederik P Kingma and Jimmy Ba. Adam: A method for stochastic optimization. *International Conference for Learning Representations*, 2015.

Thomas N Kipf and Max Welling. Semi-supervised classification with graph convolutional networks. In *International Conference for Learning Representation*, 2017.

Elyor Kodirov, Tao Xiang, and Shaogang Gong. Semantic autoencoder for zero-shot learning. In *Proceedings of the IEEE Conference on Computer Vision and Pattern Recognition*, pp. 3174–3183, 2017.

Hugo Larochelle, Dumitru Erhan, and Yoshua Bengio. Zero-data learning of new tasks. In *Proceedings of the 23rd national conference on Artificial intelligence-Volume 2*, pp. 646–651. AAAI Press, 2008.

Qimai Li, Zhichao Han, and Xiao-Ming Wu. Deeper insights into graph convolutional networks for semi-supervised learning. In *Proceedings of the 33rd national conference on Artificial intelligence*. AAAI Press, 2018.

Yanan Li, Donghui Wang, Huanhang Hu, Yuetan Lin, and Yueting Zhuang. Zero-shot recognition using dual visual-semantic mapping paths. In *Proceedings of the IEEE Conference on Computer Vision and Pattern Recognition*, 2017.

Yang Long, Li Liu, Ling Shao, Fumin Shen, Guiguang Ding, and Jungong Han. From zero-shot learning to conventional supervised classification: Unseen visual data synthesis. In *Proceedings of the IEEE Conference on Computer Vision and Pattern Recognition*, 2017.

Yao Lu. Unsupervised learning on neural network outputs: with application in zero-shot learning. In *Proceedings of the Twenty-Fifth International Joint Conference on Artificial Intelligence*, pp. 3432–3438. AAAI Press, 2016.

Thomas Mensink, Jakob Verbeek, Florent Perronnin, and Gabriela Csurka. Metric learning for large scale image classification: Generalizing to new classes at near-zero cost. In *Proceedings of the European Conference on Computer Vision*, pp. 488–501. Springer, 2012.

Ishan Misra, Abhinav Gupta, and Martial Hebert. From red wine to red tomato: Composition with context. In *Proceedings of the IEEE Conference on Computer Vision and Pattern Recognition*, pp. 1792–1801, 2017.

Mohammad Norouzi, Tomas Mikolov, Samy Bengio, Yoram Singer, Jonathon Shlens, Andrea Frome, Greg S Corrado, and Jeffrey Dean. Zero-shot learning by convex combination of semantic embeddings. *International Conference for Learning Representation*, 2014.

Mark Palatucci, Dean Pomerleau, Geoffrey E Hinton, and Tom M Mitchell. Zero-shot learning with semantic output codes. In *Advances in Neural Information Processing Systems*, pp. 1410–1418, 2009.

Adam Paszke, Sam Gross, Soumith Chintala, Gregory Chanan, Edward Yang, Zachary DeVito, Zeming Lin, Alban Desmaison, Luca Antiga, and Adam Lerer. Automatic differentiation in pytorch. In *Advances in Neural Information Processing Systems Workshop*, 2017.

Jeffrey Pennington, Richard Socher, and Christopher Manning. Glove: Global vectors for word representation. In *Proceedings of the Conference on Empirical methods in Natural Language Processing*, pp. 1532–1543, 2014.

Marcus Rohrbach, Michael Stark, and Bernt Schiele. Evaluating knowledge transfer and zero-shot learning in a large-scale setting. In *Computer Vision and Pattern Recognition (CVPR), 2011 IEEE Conference on*, pp. 1641–1648. IEEE, 2011.

Bernardino Romera-Paredes and Philip Torr. An embarrassingly simple approach to zero-shot learning. In *International Conference on Machine Learning*, pp. 2152–2161, 2015.

Ruslan Salakhutdinov, Antonio Torralba, and Josh Tenenbaum. Learning to share visual appearance for multiclass object detection. In *Computer Vision and Pattern Recognition (CVPR), 2011 IEEE Conference on*, pp. 1481–1488. IEEE, 2011.

Richard Socher, Milind Ganjoo, Christopher D Manning, and Andrew Ng. Zero-shot learning through cross-modal transfer. In *Advances in Neural Information Processing Systems*, pp. 935–943, 2013.

Nitish Srivastava, Geoffrey Hinton, Alex Krizhevsky, Ilya Sutskever, and Ruslan Salakhutdinov. Dropout: A simple way to prevent neural networks from overfitting. *The Journal of Machine Learning Research*, 15(1):1929–1958, 2014.

Xiaolong Wang, Yufei Ye, and Abhinav Gupta. Zero-shot recognition via semantic embeddings and knowledge graphs. In *The IEEE Conference on Computer Vision and Pattern Recognition (CVPR)*, June 2018.

A QUALITATIVE RESULTS

Figure 4 and 5 provide further qualitative results of our finetuned Graph Propagation Module GPM and Dense Graph Propagation Module DGP compared to a standard ResNet and GCNZ, our reimplementation of Wang et al. (2018).

ResNet: upright, grand piano, organ, accordion, barbershop
GCNZ: piano, spinet, keyboard instrument, concert grand, **baby grand**
SGCN: piano, spinet, concert grand, **baby grand**, keyboard instrument
DGP: piano, **baby grand**, concert grand, spinet, keyboard instrument

ResNet: breakwater, aircraft carrier, seashore, wing, sandbar
GCNZ: barrier, **bar**, shore, grate, geological formation
SGCN: littoral, **bar**, seaside, barrier, landfall,
DGP: **bar**, littoral, shore, seaside, landfall

ResNet: lemon, orange, banana, spaghetti squash, fig
GCNZ: **bitter orange**, temple orange, citrus, sweet orange, edible fruit
SGCN: citrus, **bitter orange**, temple orange, sweet orange, edible fruit,
DGP: citrus, **bitter orange**, sweet orange, temple orange, edible fruit

ResNet: lycaenid, cabbage butterfly, ringlet, sulphur butterfly, damselfly
GCNZ: pierid, small white, large white, hairstreak, southern cabbage butterfly
SGCN: **blue**, hairstreak, copper, pierid, butterfly,
DGP: **blue**, hairstreak, copper, pierid, butterfly

ResNet: candle, altar, lighter, lipstick, perfume
GCNZ: vigil light, rushlight, **chandlery**, dip, lamp
SGCN: vigil light, rushlight, **chandlery**, dip, high altar
DGP: vigil light, **chandlery**, rushlight, dip, flambeau

ResNet: bagel, french loaf, cheeseburger, dough, hotdog
GCNZ: onion bagel, bun, loaf of bread, **cracker**, bread dough
SGCN: onion bagel, bun, bread dough, pastry, sandwich
DGP: bun, onion bagel, bread dough, **cracker**, pastry

ResNet: walking stick, jacamar, hip, house finch, chainlink fence
GCNZ: **diapheromera**, phasmid, finch, oscine, praying mantis
SGCN: **diapheromera**, phasmid, neuropteron, thrush, finch
DGP: **diapheromera**, phasmid, thrush, titmouse, oscine

Figure 4: Qualitative result comparison on Imagenet. The correct class is highlighted in bold. We report the top-5 classification results.

ResNet: desktop computer, monitor, screen, computer keyboard, mouse
GCNZ: personal computer, portable computer, planner, computer, computer screen
SGCN: personal computer, computer, computer screen, **display**, television monitor
DGP: personal computer, background, computer screen, portable computer, **display**

ResNet: bittern, partridge, coucal, ruffed grouse, kite
GCNZ: least bittern, american bittern, **european bittern**, phasianid, crow pheasant
SGCN: american bittern, **european bittern**, least bittern, plain turkey, great bustard
DGP: american bittern, least bittern, **european bittern**, heron, egret

ResNet: damselfly, dragonfly, lacewing, walking stick, grasshopper
GCNZ: **odonate**, neuropteron, hymenopterous insect, phasmid, brown lacewing
SGCN: **odonate**, neuropteron, brown lacewing, green lacewing, phasmid
DGP: **odonate**, brown lacewing, green lacewing, neuropteron, phasmid

ResNet: macaw, lorikeet, bee eater, sulphur-crested cockatoo, house finch
GCNZ: lory, **parrot**, rainbow lorikeet, varied lorikeet, cockatoo
SGCN: **parrot**, lory, rainbow lorikeet, varied lorikeet, cockatoo
DGP: lory, **parrot**, cockatoo, rainbow lorikeet, varied lorikeet

ResNet: grocery store, confectionery, tobacco shop, restaurant, butcher shop
GCNZ: marketplace, greengrocery, **supermarket**, shop, tuck shop
SGCN: **supermarket**, marketplace, greengrocery, tuck shop, shop
DGP: **supermarket**, greengrocery, marketplace, tuck shop, shop

ResNet: cliff, valley, lakeside, alp, promontory
GCNZ: geological formation, natural elevation, natural depression, mountain, ravine
SGCN: **precipice**, crag, natural depression, ravine, natural elevation
DGP: natural depression, geological formation, natural elevation, crag, **precipice**

ResNet: church, monastery, dome, bell cote, mosque
GCNZ: kirk, cathedral, abbey, basilica, cathedral
SGCN: abbey, cathedral, friary, basilica, cathedral
DGP: cathedral, abbey, cathedral, basilica, kirk

true label: **place of worship**

Figure 5: Qualitative result comparison on Imagenet. The correct class is highlighted in bold. We report the top-5 classification results.

B TWO-PHASE PROPAGATION

Table 5 illustrates the benefit of a two-phase directed propagation rule where ancestors and descendants are considered individually compared to two consecutive updates using the full adjacency matrix in the dense method.

Table 5: Results for 2-hops with/without separating the adjacency matrix into ancestors and descendants for DGP.

Model	**Hit@k (%)**				
	1	2	5	10	20
without	26.0	40.2	59.8	71.4	80.3
with	**26.6**	**40.7**	**60.3**	**72.3**	**81.3**

C ANALYSIS OF NUMBER OF LAYERS

Table 6 illustrates the drop in performance that is caused by using additional hidden layers in the GCN for the 2-hops experiment. All hidden layers have dimensionality of 2048 with 0.5 dropout.

Table 6: Results for 2-hops for SGCN with increasing depth.

#Layers	**Hit@k (%)**				
	1	2	5	10	20
1	**24.8**	**38.3**	**57.5**	**69.9**	**79.6**
2	24.2	37.7	57.4	69.2	78.1
3	23.9	37.5	57.1	68.4	77.2

D PERFORMANCE IMPROVEMENTS BETWEEN GCNZ AND SGCN

Table 7 explains the performance difference between our SGCN, our reimplementation of GCNZ and the reported results in Wang et al. (2018). Note, unless otherwise stated training is performed for 3000 epochs. Non-symmetric normalization ($D^{-1}A$) is denoted as *non-sym* in the normalization column, while a symmetric normalization ($D^{-1/2}AD^{-1/2}$) is denoted as *sym*. No finetuning has been performed for SGCN in these results.

Table 7: Illustration of the improvements between the original results of GCNZ in Wang et al. (2018), our reimplementation of GCNZ and our SGCN.

Model	Norm	**Hit@k (%)**				
		1	2	5	10	20
GCNZ (300 epochs) (Wang et al., 2018)	sym	19.8	33.3	53.2	65.4	74.6
GCNZ (300 epochs) (Wang et al., 2018)[a]	sym	21.0	33.7	52.7	64.8	74.3
GCNZ (ours) (300 epochs)	sym	21.4	34.7	54.3	67.5	77.6
GCNZ (ours)	sym	23.5	36.9	56.5	68.8	78.0
SGCN (ours)	sym	24.6	38.1	57.6	70.0	79.7
SGCN (ours)	non-sym	24.8	38.3	57.5	69.9	79.6

[a]Updated results from Wang et al. (2018) `https://github.com/JudyYe/zero-shot-gcn`

E ROBUSTNESS OF RESULTS

Table 8 shows the mean and std for 3 runs for the 2-hops and All dataset. It can clearly be observed that as the number of classes increases (2-hops to all), results become more stable.

Table 8: Mean and std for 3 runs. More stable as # class increases.

Test set	**Model**	**Hit@k (%)**	
		1	2
2-hops	SGCN	26.17±0.03	40.41±0.03
	DGP	26.67±0.09	40.74±0.04
All	SGCN	2.80±0.01	4.90±0.01
	DGP	2.95±0.00	5.05±0.02